



## **The Role of the Anion in Concentrated Electrolytes for Lithium-Sulfur Batteries**

Downloaded from: <https://research.chalmers.se>, 2025-12-04 22:50 UTC

Citation for the original published paper (version of record):

Kottarathil, A., Slim, Z., Ahmad Ishfaq, H. et al (2024). The Role of the Anion in Concentrated Electrolytes for Lithium-Sulfur Batteries. *Journal of the Electrochemical Society*, 171(7).  
<http://dx.doi.org/10.1149/1945-7111/ad5b8c>

N.B. When citing this work, cite the original published paper.

OPEN ACCESS

# The Role of the Anion in Concentrated Electrolytes for Lithium-Sulfur Batteries

To cite this article: Aginmariya Kottarathil *et al* 2024 *J. Electrochem. Soc.* **171** 070506




View the [article online](#) for updates and enhancements.

## You may also like

- [Polymer electrolytes for metal-ion batteries](#)  
Daria Yu. Voropaeva, Svetlana A. Novikova and Andrey B. Yaroslavtsev
- [Review—Superconcentrated Electrolytes for Lithium Batteries](#)  
Yuki Yamada and Atsuo Yamada
- [Insights into the use of polyethylene oxide in energy storage/conversion devices: a critical review](#)  
Anil Arya and A L Sharma



# The Role of the Anion in Concentrated Electrolytes for Lithium-Sulfur Batteries

Aginmariya Kottarathil,<sup>1,2,3</sup>  Zaher Slim,<sup>2</sup> Hafiz Ahmad Ishfaq,<sup>2,3,4</sup> Steffen Jeschke,<sup>5</sup> Grażyna Zofia Żukowska,<sup>1</sup> Maciej Marczewski,<sup>1</sup> Katarzyna Lech,<sup>1</sup> Patrik Johansson,<sup>2,3</sup>  and Władysław Wiczorek<sup>1,3,z</sup> 

<sup>1</sup>Warsaw University of Technology, Faculty of Chemistry, 00664, Warszawa, Poland

<sup>2</sup>Chalmers University of Technology, Department of Physics, 412 96, Gothenburg, Sweden

<sup>3</sup>Alistore-ERI, CNRS FR 3104, 80039 Amiens, France

<sup>4</sup>National Institute of Chemistry Hajdrihova 19, 1000 Ljubljana, Slovenia

<sup>5</sup>Centre for Catalysis and Clean Energy, School of Environment and Science, Griffith University, Gold Coast campus QLD 4215, Australia

Highly concentrated electrolytes show promise in enhancing lithium-sulfur (Li-S) battery performance by mitigating polysulfide (PS) solubility. The role of the salt anion for the performance improvement(s) is however not well understood. Here a systematic characterization using (concentrated) electrolytes based on three different salts: LiTFSI, LiTf, and LiTDI, in a common DOL:DME solvent mixture is reported for a wide range of physicochemical and electrochemical properties: ionic conductivity, density, viscosity, speciation, and PS solubility. While increased salt concentration in general improves Li-S battery performance, the role of the salt anion introduces complexity. The 2 m LiTDI-based electrolyte, with a slightly higher viscosity and lower PS solubility, outperforms the LiTFSI-based counterpart in terms of accessible reversible capacity. Conversely, the 2 m LiTf-based electrolyte exhibits subpar performance due to the formation of ionic aggregates that renders more free solvent and, therefore higher PS solubility, which, however can be improved by using a 5 m concentrated electrolyte. Hence, using electrolyte salt concentration as a rational design route demands an understanding of the local molecular structure, largely determined/affected by the choice of anion, as well as how it connects to the global properties and in the end improved Li-S battery performance.

© 2024 The Author(s). Published on behalf of The Electrochemical Society by IOP Publishing Limited. This is an open access article distributed under the terms of the Creative Commons Attribution 4.0 License (CC BY, <http://creativecommons.org/licenses/by/4.0/>), which permits unrestricted reuse of the work in any medium, provided the original work is properly cited. [DOI: 10.1149/1945-7111/ad5b8c]



Manuscript submitted March 11, 2024; revised manuscript received May 25, 2024. Published July 4, 2024.

Supplementary material for this article is available [online](#)

The ever-increasing demands for renewable energy storage devices and the pressing need to electrify the transportation system necessitate the development of new battery concepts.<sup>1,2</sup> Lithium-ion batteries are based on intercalation-type cathodes.<sup>3</sup> However, cathodes based on conversion-type redox chemistry can offer exceptionally high volumetric and gravimetric capacities.<sup>4–6</sup> In this context, lithium-sulfur (Li-S) batteries are gaining considerable attention.<sup>7–10</sup> By combining sulfur that has a high theoretical specific capacity (1672 mAh g<sup>−1</sup>) with a lithium metal anode, specific cell energy densities as high as 500–600 Wh kg<sup>−1</sup> can be realised.<sup>10</sup> The natural abundance of elemental sulfur and its low cost means that the life cycle impact of Li-S batteries on the environment will be relatively low.<sup>10,11</sup> However, the practical application of Li-S batteries is hindered by both capacity fading and lithium dendrite formation upon cycling.<sup>5,12</sup> Additionally, the redox reactions at the cathode result in the formation of polysulfides (PSs) that lead to the loss of active material. As these PSs migrate from the cathode to the electrolyte, they react with the lithium metal anode to form an insulating layer, which increases the cell impedance.<sup>13,14</sup> The presence of soluble PSs and sulfur also causes lithium corrosion.<sup>15</sup> Limiting PS solubility is therefore expected to significantly improve Li-S cell cycle life by suppressing the shuttle mechanism, reducing the anode contamination and minimizing the cathode active material loss.<sup>16</sup> Several strategies have been devised to overcome the limitations of Li-S batteries. For instance, to address the high capacity fading problem, carbon cathode architectures such as porous carbon, carbon nanotubes, and graphene can be used to confine the PS.<sup>17,18</sup> To suppress the reaction between lithium metal anode and PS, additives such as lithium nitrate (LiNO<sub>3</sub>) can be used. LiNO<sub>3</sub> also forms a stable solid-electrolyte interphase (SEI) (a protective layer) on the lithium metal anode.<sup>7</sup> However, it cannot prevent the dissolution of PSs into the electrolyte, leading to long-

term cycling instability.<sup>19</sup> Similarly, inorganic solid electrolytes prevent the reaction between soluble PSs and the lithium metal anode by forming a protective layer.<sup>20</sup> However, the brittleness of such inorganic solid electrolyte materials limits their application in large-surface practical systems.<sup>19,21</sup> Alternatively, lithium metal anode can be protected by coating with protective layers or by creating an artificial SEI.<sup>22,23</sup>

The PS dissolution and migration can also possibly be prevented by using highly concentrated electrolytes (HCEs).<sup>24</sup> HCEs, also known as “solvent-in-salt”<sup>21</sup> electrolytes and similar to “polymer-in-salt”<sup>25,26</sup> electrolytes can be used to limit the solubility of PSs.<sup>27–29</sup> In these electrolytes, the Li<sup>+</sup> cations in general coordinate more to the anions than to the solvent molecules, and simultaneously, there is a decrease in free solvent, both improving the performance of Li-S batteries.<sup>24,30</sup> Moreover, the increased concentration of Li<sup>+</sup> cations promotes a more homogeneous plating/stripping process and a robust anion-derived SEI that suppresses side reactions between the electrolyte and the lithium metal anode.<sup>31</sup> Overall, HCEs inhibit dendrite growth.<sup>32</sup> Most often, HCEs consist of conventional lithium salts (LiTFSI, LiTDI, LiTf) dissolved in organic solvents, such as mixtures of DOL and DME.<sup>33</sup> Here, LiTFSI is lithium bis(trifluoromethanesulfonyl)imide (Li[N(SO<sub>2</sub>CF<sub>3</sub>)<sub>2</sub>]), LiTDI is lithium 4,5-dicyano-2-(trifluoromethyl)imidazole (Li[C<sub>6</sub>F<sub>3</sub>N<sub>4</sub>]), LiTf is lithium trifluoromethanesulfonate (Li[SO<sub>3</sub>CF<sub>3</sub>]), DOL is 1,3-dioxolane (DOL) and DME is 1,2-dimethoxyethane (DME).

LiTFSI has been used at high concentrations in Li-S batteries by Shin et al., much due to its ability to suppress the solubility of lithium polysulfides (LiPSs) through the common ion effect.<sup>34</sup> Subsequently, the concentration of this salt was increased even further, up to 7 mol/litre of solvent, resulting in impressive performance with over 800 mAh g<sup>−1</sup> and close to 100% coulombic efficiency.<sup>21</sup> Equimolar mixtures of glymes with lithium salts such as LiTFSI and LiTf have also been investigated in Li-S batteries. The former, termed solvate ionic liquid, results in low PS solubility, while the latter, a concentrated electrolyte with high ionic association strength renders high PS solubility.<sup>27,35</sup> Another reason for the popularity of LiTFSI

<sup>z</sup>E-mail: [wladyslaw.wiczorek@pw.edu.pl](mailto:wladyslaw.wiczorek@pw.edu.pl)

and LiTf for HCEs is their high thermal stabilities and compatibility with the ether solvents.<sup>33,36</sup> In particular, LiTFSI is highly dissociated in DOL:DME, while LiTDI is a Hückel anion-based salt<sup>37</sup> that has weak interaction with polysulfides.<sup>16,38</sup>

Though HCEs have many advantages, many challenges still limit the application of HCEs. HCEs, apart from being expensive due to large amounts of salts, also have high viscosities and low ionic conductivities.<sup>39</sup> The high viscosity of HCEs can extend their wetting time compared to conventional electrolytes if a similar manufacturing process is used.<sup>39</sup> To improve the cyclability and overall performance of HCEs, a better understanding of physicochemical properties of these electrolytes is required.

Previous research has explored concentrated LiTFSI-based electrolytes ranging from 1 to 7 mol/litre<sup>21</sup> and LiTf-based ones up to 3 mol/litre, while for LiTDI-based electrolytes the salt concentration has been limited to 1 mol/litre.<sup>40</sup> In contrast, we here combine experimental and computational approaches to investigate electrolytes based on LiTFSI, LiTDI, and LiTf dissolved in a binary solvent mixture of DOL:DME (1:1, v/v) up to each and every system's maximum salt solubility. We aim to provide fundamental structural and mechanistic insights into the role of the lithium salt anion in different HCEs and less concentrated electrolytes. The physicochemical properties and electrochemical battery performance are rationalised using local structure analysis and speciation, including PS solubility.

## Experimental and Computational Methods

**Materials and electrolyte preparation.**—LiTDI was synthesised as reported previously.<sup>37</sup> LiTFSI (99.9%) was purchased from Solvionic, while LiTf (99.8%), DOL (99.8%), DME (99.8%) and elemental sulfur (99.8%) were all purchased from Sigma-Aldrich. The salts were dried at 140°C under vacuum overnight before use. All salts and solvents were handled in an argon-filled glove box at all times (< 1 ppm H<sub>2</sub>O). The electrolytes were made by preparing a DOL:DME (1:1, v/v) solvent mixture and dissolving (using a magnetic stirrer for 24 h at room temperature) appropriate amounts of salts to get the desired concentrations, i.e., 1–7 m LiTFSI, 1–2 m LiTDI, and 1–5 m LiTf. The highest concentrations are based on the maximum salt solubilities (here, 1 m refers to 1 mole of salt per litre of solvent and the solvent to salt mole ratios are given in Table S1, Supplementary Information).

**Raman spectroscopy.**—The samples for the Raman spectroscopy measurements were 0.5–1 cm<sup>3</sup> and sealed in 4 cm<sup>3</sup> glass vials. The spectra were collected on a Nicolet Almega Raman dispersive spectrometer using a diode laser with an excitation wavelength of 532 nm and a spectral resolution of 2 cm<sup>−1</sup>. The deconvolution of the spectra was done using the OMNIC software (OMNIC, Thermo Scientific) and using Voigt functions.

**Physicochemical and electrochemical properties.**—The densities and viscosities were recorded for 10–50 °C at an interval of 10 °C using an Anton Paar DMA4500M density meter equipped with a Lovis 2000M rolling ball viscometer module. The temperature accuracy was 0.02 °C and it took approximately 5 min to reach equilibrium. The viscosity values were obtained by averaging the results from at least 5 back-and-forth runs of the rolling ball. Prior to the measurements, the instrument was calibrated and verified using standards. The ionic conductivities were measured for 0–50 °C at an interval of 10 °C, with a thermal equilibration of at least 30 min, using electrochemical impedance spectroscopy with an A.C. signal of 5 mV in 500 kHz to 10 Hz range with 10 points per decade on a VMP3 instrument from Bio-Logic. Electrolytes were placed into micro conductivity cells with cell constants values = 0.3–0.7 cm<sup>−1</sup>, which were then put into a cryostat-thermostat system (Haake K75 with the DC50 temperature controller).

**Li-S battery tests.**—Stepping through the electrochemical cell materials and components, the anode lithium metal foil was 200 μm

thick (Toyota Tsusho), while the C/S composite cathode was composed of sulfur with 60 wt% sulfur loading (Sigma-Aldrich, 99.998% trace metal basis), carbon black (Vulcan) as conductive additive, 38.5 wt%, and sodium carboxymethyl cellulose (Na-CMC, Mw = 700,000, Sigma-Aldrich) as binder, 1.5 wt%. To prepare the electrodes, appropriate quantities of sulfur and carbon black were mixed in mortar. Next, the binder was added, and the solution was mixed magnetically to obtain a homogenous slurry. The electrode suspension was cast on a 20 μm aluminum foil (Hohsen) using the Doctor Blade technique, resulting in a coating with a thickness of 250 μm. After coating, the electrode was dried at 60 °C under vacuum for 24 h. The coin cells (CR2032) were assembled inside the argon-filled glove box, with a C/S composite cathode (13 mm), a lithium metal foil anode (14 mm), and a Whatman glass fibre filter (16 mm) separator. A 20–25 μL mgS<sup>−1</sup> ratio was chosen to ensure adequate wetting of the separator for the HCEs. The Whatman glass fiber was used similar to previous work.<sup>21</sup> The coin cells were cycled using a Scribner Associates Incorporated 580 Battery Test System between 1–3 V vs. Li<sup>+</sup>/Li<sup>0</sup>. The initial cycle was run at C/30, and thereafter, the cycling was made at C/10 (1 C=1672 mAh g<sup>−1</sup>S).

**High-performance liquid chromatography.**—The method/protocol for the high-performance liquid chromatography with spectrophotometric detection (HPLC-DAD) experiments was based on the literature.<sup>41</sup> A 5.46 mM stock solution was prepared by dissolving 0.007 g elemental sulfur in 5 mL DME. The stock solution was then diluted to provide the standard solutions of 2.184 mM, 0.4368 mM, 0.0873 mM and 0.0174 mM (Fig. S1, Supplementary Information). The elemental S saturated solutions were made by dissolving 0.1 g of elemental S into a sample vial with 2.5 mL of target electrolyte or suitable solvent. After being sealed and shaken for 96 h, the solution was allowed to rest for 72 h; the clear solution at the top was used for the analysis. An Agilent 1100 quaternary pump (from Agilent Technologies) was used to deliver 100% methanol of LC-MS grade (POCH, Gliwice, Poland) through an HPLC column Zorbax SB-C18 (from Agilent Technologies, 4.6 × 150 nm, 3.5 μm) with an analogous precolumn at flow rate 0.5 mL/min using an isocratic elution. A 7725i Rheodyne manual injector was used to inject 20 μL of each sample, and a 1100 diode array detector (DAD) from Hewlett-Packard with spectrophotometric detection was operated at 219 and 264 nm, and a total HPLC running time of 12 min. UV spectra were collected in the 200–300 nm range.

**Computational studies.**—The conductor-like screening model for real solvents (COSMO-RS)<sup>42,43</sup> was used to predict the solubility of Li<sub>2</sub>S<sub>8</sub> in the electrolytes.<sup>44</sup> The COSMO-RS calculations were conducted using the COSMOthermX program<sup>45</sup> and the BP-TZVPD-C30-1701 parameterization at a temperature of 293.15 K. The TURBOMOLE V7.1 software package<sup>46</sup> was used to initially optimise the geometries of the molecules using density functional theory (DFT)<sup>47,48</sup> using the BP86 functional and the TZVP basis set in both the gas phase and assuming a perfect conductor ( $\epsilon = \infty$ ). Additionally, single-point calculations were performed using BP86/TZVPD to generate a fine grid cavity. The molecular structures and cosmo-files for TFSI, Tf, TDI, DOL and DME were obtained using the TmolX 4.6.0 graphical user interface and were added to the COSMOthermX database.

All COSMO-RS computations were performed for all concentrations of the electrolytes made with LiTFSI and LiTDI in DOL:DME (1:1, v/v) using mole fractions. The Li<sub>2</sub>S<sub>8</sub> solubility was predicted using combined machine learning-approaches with COSMO-RS descriptors based on previous work.<sup>44</sup>

## Results and Discussion

Initially, we prepared a series of electrolytes by dissolving appropriate amounts of LiTFSI, LiTf and LiTDI (Fig. 1) in DOL:DME (1:1, v/v). Subsequently, we conducted a detailed analysis of the speciation (“free” anions, ion-pairs, and aggregates) in these

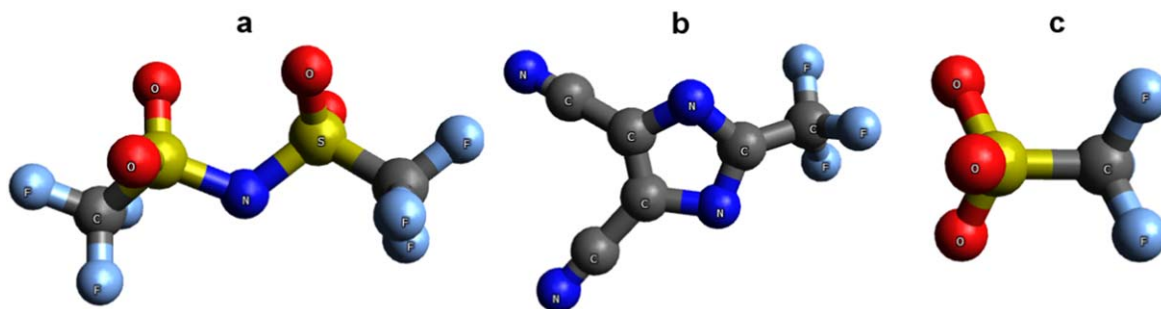


**Figure 1.** Chemical structures of the anions (a) TFSI (bis(trifluoromethanesulfonyl)imide), (b) TDI (4,5-dicyano-2-(trifluoromethyl)imidazole), and (c) Tf (trifluoromethanesulfonate).

electrolytes for various salt concentrations, with special emphasis on the role of the different anions/salts. Then findings were connected to the physicochemical properties and ionicities to further understand these properties, alongside elemental sulfur and  $\text{Li}_2\text{S}_8$  solubilities via both HPLC measurements and COSMO-RS modelling, affect Li-S battery performance.

**Local structure, speciation and ion transport.**—The electrochemical performance of an electrolyte depends on its physicochemical properties, such as local structure and speciation, ionic conductivity and viscosity. The local structure and speciation i.e., “free” anions, ion-pairs, and aggregates.<sup>49,50</sup> In HCEs, the interaction between the  $\text{Li}^+$  cations and the anions leads to the formation of ion-pairs (solvent-separated or contact ion-pairs) and aggregates,<sup>51</sup> which can be semi-quantitatively determined by deconvolution of the electrolyte Raman spectra (Fig. 2 and Fig. S2).

For all three electrolytes at standard 1 m concentrations, we observe a band of “free” anions at  $739\text{ cm}^{-1}$  for LiTFSI (Fig. 2a), at  $2227\text{ cm}^{-1}$  (Fig. 2b) and at  $977\text{ cm}^{-1}$  (Fig. S3a) for LiTDI and at  $757\text{ cm}^{-1}$  (Fig. 2c) and at  $1032\text{ cm}^{-1}$  (Fig. S3b) for LiTf.<sup>49</sup> The presence of these “free” anions can be rationalised using Debye-Hückel theory, which explains that as the electrostatic interactions decrease, the concentration of “free” ions increases.<sup>51</sup> As the salt concentration increases, we observe band splitting and a gradual shift toward higher frequencies (Fig. 2a–c), signatures of an increase in ion-pairs and aggregates and a decrease in “free” anions in line with previous reports.<sup>49,51,53,55</sup> For the different electrolytes at the same 2 m concentration, i.e., different anions/salts, the trend in “free” anions is: LiTFSI > LiTDI > LiTf (Fig. 2d and Table S2).

These trends and hence the ionic association strength of the anions, depend on the charge delocalization within the anion.<sup>51</sup> Anions can also be considered as Lewis bases with donor numbers (DNs).<sup>36</sup> A strong Lewis base interacts more strongly with a strong Lewis acid, such as a  $\text{Li}^+$  cation. In particular, for LiTFSI, the large concentration of “free” anions indicates higher ionic dissociation and hence more  $\text{Li}^+$  cation-solvent coordination, that in turn leads to less free solvent present. This agrees with TFSI being a relatively weak Lewis base ( $\text{DN} = 5.4\text{ kcal mol}^{-1}$ ) and interacts weakly with the  $\text{Li}^+$  cations. LiTDI is in many ways intermediate between LiTFSI and LiTf, and we observe the presence of ion-pairs and aggregates in the 2 m LiTDI electrolyte.<sup>56</sup> For LiTf, less “free” anions indicate less ionic dissociation and hence less  $\text{Li}^+$  cation-solvent interactions, leading to more “free” solvent as also seen in Fig. S4. The Tf anion is a strong Lewis base ( $\text{DN} = 16.9\text{ kcal mol}^{-1}$ ) and therefore interacts strongly with the  $\text{Li}^+$  cations.<sup>56</sup>

The Li-S battery performance also depends on the ionic conductivity and viscosity, and in general, the former decreases and the latter increases as a function of salt concentration (Fig. 3a). For a common 2 m salt concentration, the trend in ionic conductivity is: LiTFSI > LiTDI > LiTf, which is similar to the trend for “free” anions. However, the viscosity is not inversely proportional to the ionic conductivity, as one might expect (Fig. 3a);  $\text{LiTDI} \approx \text{LiTFSI} > \text{LiTf}$  (Table S2). The low ionic conductivity of the LiTf-based

electrolyte can be explained by the extensive ionic association and the low viscosity can be rationalised by a large amount of free solvent<sup>57</sup> evident from the Raman spectra (Fig. S4). As the LiTf salt concentration increases from 1 m to 3 m, the viscosity does not increase significantly (viscosity < 5 mPa.s). However, the viscosity increases significantly at 5 m, to 16.4 mPa.s. For LiTFSI (1–7 m), the situation is quite different; the viscosity increases from 1.15 mPa.s to a vast 225 mPa.s, while the ionic conductivity decrease is much less pronounced (Fig. 3a).

Furthermore, to assess the ionicity, we analyse the Walden plot (Fig. 3b) that depicts the relation between transport properties, including the molar conductivity ( $\lambda$ ) and the fluidity ( $\eta$ ), the reciprocal of viscosity.<sup>58,59</sup> Here, the observations at different temperatures (10–50 °C) for the same electrolyte family show that as the salt concentration increases, the ionicity decreases (Fig. 3b). For the 2 m concentration electrolytes, the trend in ionicity is: LiTFSI > LiTDI > LiTf, which is similar to the trend for “free” anions and ionic conductivity. At very high salt concentrations, as for 7 m LiTFSI, the electrolyte approaches the superionic region, which also can be correlated with a report on high transference numbers (0.73) for this specific electrolyte.<sup>21</sup> The ion transport mechanism in HCEs differs from that in conventional dilute electrolytes depending on the  $\text{Li}^+$ -coordination with surrounding ions. In dilute/conventional electrolytes, a vehicular ion-conduction mechanism prevails, i.e. the  $\text{Li}^+$  cations move with their solvation shells while the non-coordinated or “free” anions exhibit long lifetimes.<sup>60,61</sup> In HCEs, the  $\text{Li}^+$  cations move in concerted aggregated motions, hops, or exchanges their solvent shells, phenomena described as structural diffusion,<sup>59,62</sup> or as non-vehicular/exchange mechanisms,<sup>63</sup> as for example reported to occur for sulfolane and acetonitrile-based HCEs.<sup>31,64</sup>

**Electrochemical performance.**—The electrochemical performance tests using the different electrolytes did not comprise the 4–7 m LiTFSI electrolytes as these are already reported in the literature for the same solvent mixture (DOL:DME, 1:1, v/v).<sup>21,34</sup> For all cells, during the first discharge, we observe a plateau at 2.3–2.4 V which is the elemental sulfur ( $\text{S}_8$ ) accepting electrons to form long chain PS  $\text{Li}_2\text{S}_x$  ( $x = 6-8$ ), and subsequently a plateau at 2.1 V, which corresponds to the reduction of various PS  $\text{Li}_2\text{S}_x$  to  $\text{Li}_2\text{S}_2$ .<sup>15,36</sup>

The electrochemical performance is expected to improve at higher salt concentrations. In particular the LiTFSI-based electrolytes, going from 1 m to 3 m, the discharge capacity significantly increases from  $220\text{ mAh g}^{-1}$  to  $410\text{ mAh g}^{-1}$  (Fig. 4a,b). For the LiTDI-based electrolytes, from 1 m to 2 m, the specific capacity increases from  $300\text{ mAh g}^{-1}$  to  $380\text{ mAh g}^{-1}$  (fig. 4c,d). For LiTf-based electrolytes, however, from 1 m to 3 m, we do not observe any significant increase in the specific capacity, but for the 5 m concentrated electrolyte, we observe a specific capacity of about  $230\text{ mAh g}^{-1}$  (Fig. 4e,f). This observation can indeed be correlated with the high concentration of free solvent and the low viscosity of these electrolytes, resulting in increased PS solubility.<sup>38,65</sup> The coulombic efficiency (CE) improved with increased salt concentration (Fig. S5). The lower CEs,



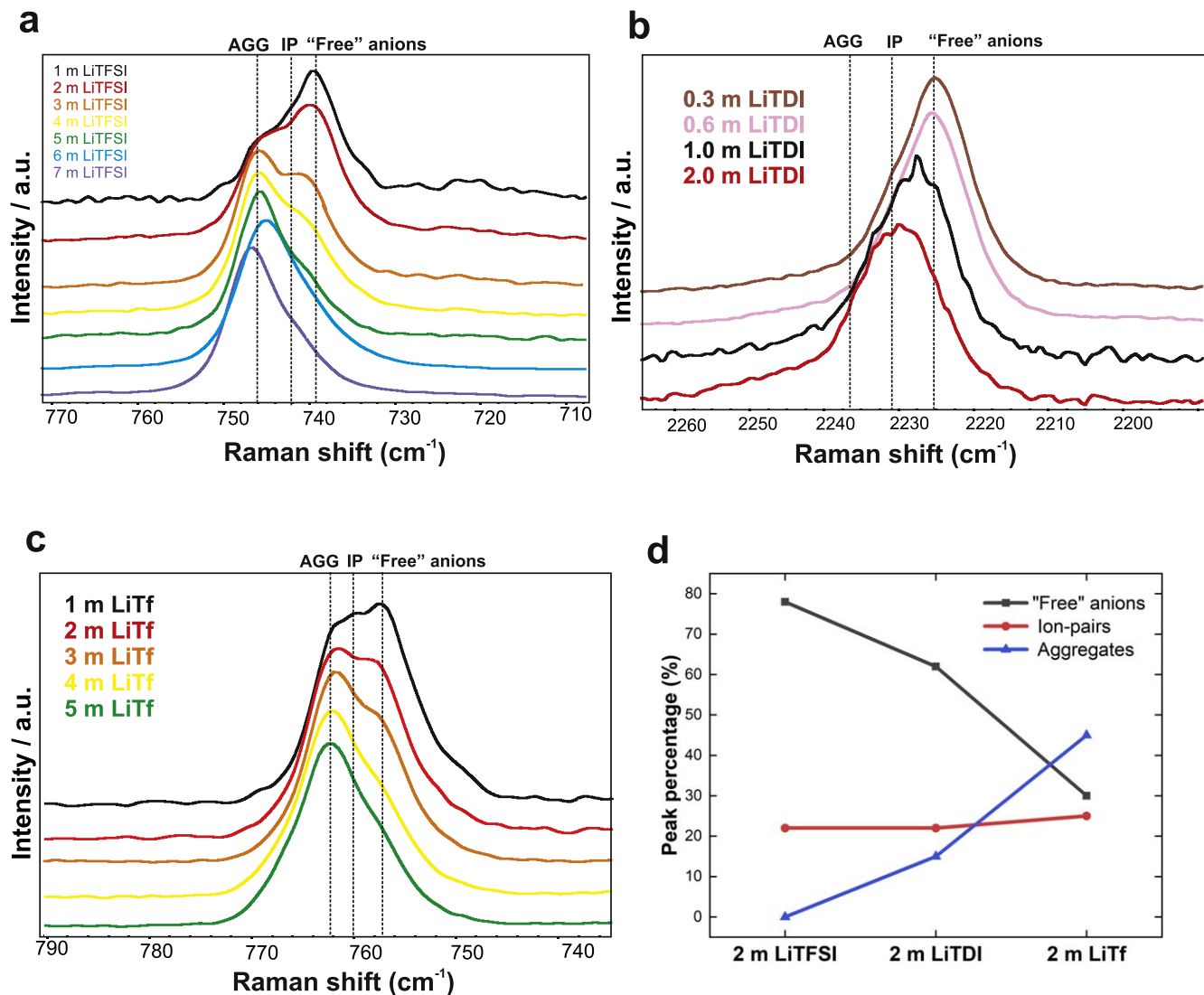


**Figure 2.** (a) Raman spectra in the  $\nu_s(\text{S-N-S})$  region for 1-7 m LiTFSI in DOL:DME (b) the  $\nu_s(\text{CN})$  bending region for 0.3-2.0 m LiTDI in DOL:DME (c) the  $\delta_s(\text{CF}_3)$  bending region for 1-5 m LiTf, and (d) Comparison of the estimated amount "free" anions, ion-pairs, and aggregates for the 2 m LiTFSI, LiTDI and LiTf in DOL:DME (1:1, v/v) electrolytes.<sup>52-55</sup>

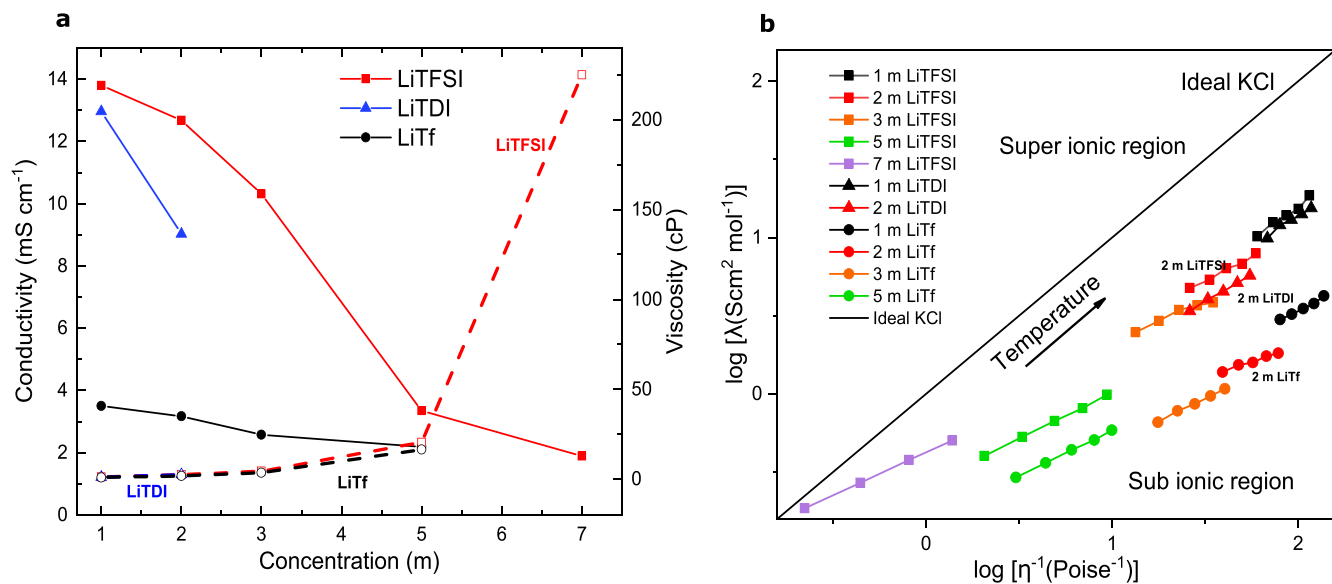


**Figure 3.** (a) Ionic conductivity and viscosity of the electrolytes at 30 °C, filled symbols are conductivity and the open ones are viscosity (b) Walden plot from temperature-dependent molar conductivities and viscosities.

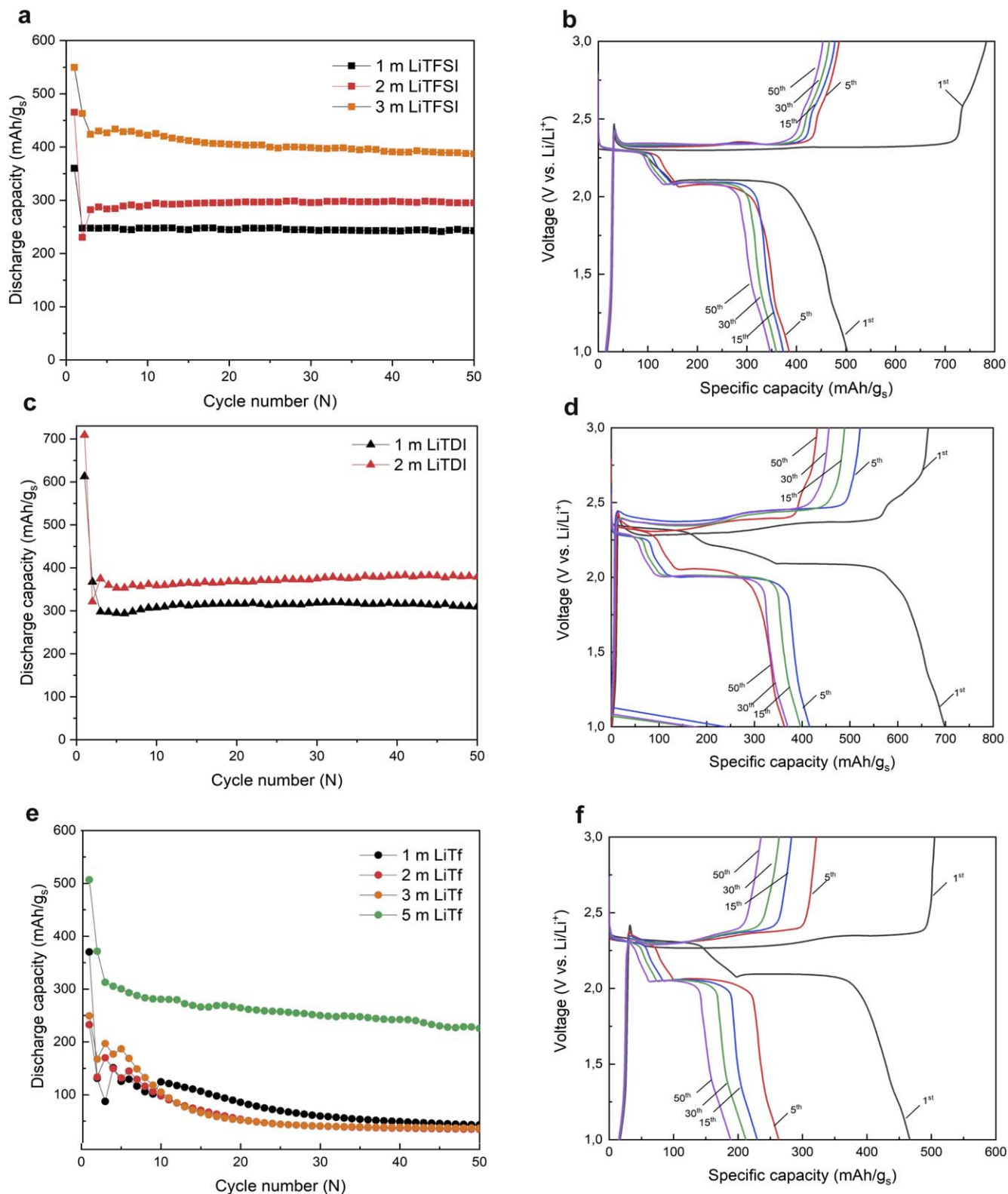


**Figure 4.** Cycling behaviour at C/10 (1st cycle C/30) for LiTFSI, LiTDI and LiTf in DOL:DME (1:1,v/v). Discharge capacity of (a) LiTFSI (1-3 m), (c) LiTDI (1-2 m) and (e) LiTf (1-5 m). Selected discharge-charge voltage profiles for the (b) 3 m LiTFSI, (d) 2 m LiTDI and (f) 5 m LiTf.

characterised by a decrease in discharge capacity and an increase in charge capacity, are attributed to the redox shuttle mechanism of PS. At lower electrolyte salt concentrations, the CE is overall notably low for the initial cycles but gradually improves, albeit with an inevitable decrease in capacity. In contrast, for higher salt concentrations, the CE remains above 80% from the initial cycles up to 50 cycles, which can

be attributed to the lower Li<sub>2</sub>S<sub>8</sub> solubility, indicating that the solid Li<sub>2</sub>S<sub>x</sub> remains in the composite cathode and undergoes a reversible redox reaction.<sup>27</sup>

For the comparative analysis of the electrolytes at the 2 m salt concentration, the discharge capacities follow: LiTDI > LiTFSI >> LiTf (Fig. 5a).

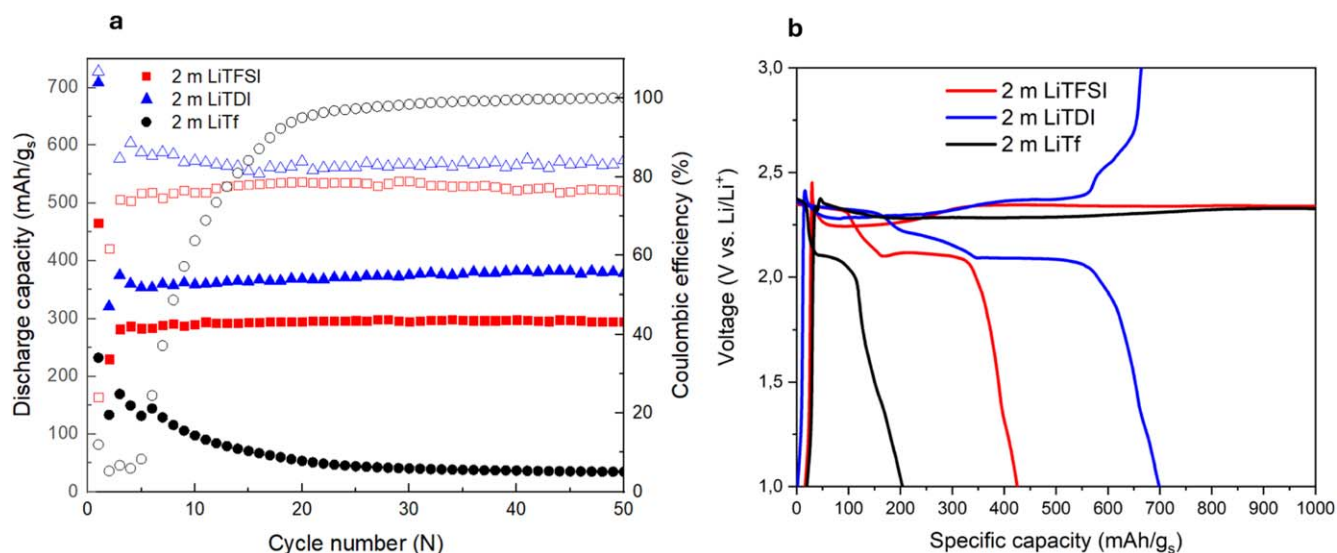


**Figure 5.** (a) Comparison of discharge capacity of 2 m LiTFSI, LiTDI, and LiTf (b) discharge-charge profiles at cycle 1 for the 2 m LiTFSI, LiTDI and LiTf-based electrolytes.

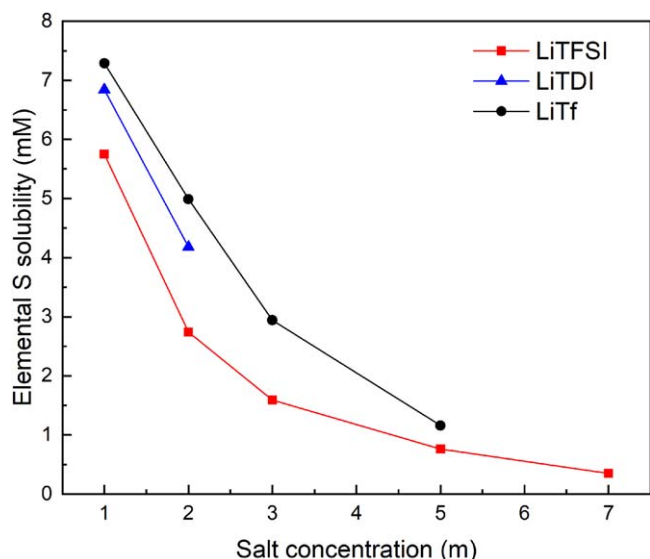


**Figure 6.** Solubility of elemental sulfur in various electrolytes using HPLC-DAD (219 nm).

The initial specific discharge capacity for LiTDI, LiTFSI, and LiTf is 710 mAh g<sup>-1</sup>, 465 mAh g<sup>-1</sup>, and 230 mAh g<sup>-1</sup>, respectively (Fig. 5b).

Note that for LiTFSI and LiTf, the initial charge capacity may be significantly higher than the discharge capacity, as compared to the LiTDI-based electrolytes. The overcharging observed for LiTFSI and LiTf are possibly due to the PS shuttle mechanism and side reactions of the lithium anode, which prevents the full discharge capacity from being regained on charging. The CEs are similar for the LiTFSI and LiTDI-based electrolytes, around 80%, while it is quite low for the LiTf-based electrolytes. Overall, we observe a slightly better electrochemical performance at 2 m salt concentration for the LiTDI-based electrolyte, which may at first glance appear surprising as the LiTFSI-based electrolyte has more “free” anions, less free solvent, and higher ionic conductivity, but the slightly higher viscosity of LiTDI alongside with its lower PS solubility (Table S1), is decisive.

**Elemental sulfur and LiPS solubility.**—To actually examine the solubility of elemental sulfur and PS, we use HPLC-DAD and

COSMO-RS modelling<sup>44</sup> (Fig. 6 and Table S1). The experimental elemental S solubility trend follows: LiTf > LiTDI > LiTFSI, which thus explains the poor performance of the LiTf-based electrolytes. Still, it does not explain the better performance of the LiTDI-based electrolytes.

The solubility of LiPS, in any electrolyte, depends on several factors, such as the Li<sup>+</sup> cation-anion interaction strength and the solvent molecular structures.<sup>66</sup> Electrolytes with stronger cation-anion interactions are expected to have higher LiPS solubility as the Li<sup>+</sup> cation interacts strongly also with the PS anion. For e.g. in the LiTf-based electrolytes, there is also abundant free solvent, due to the solvation of Li<sup>+</sup> cations by Tf anions, which in addition, as it is stronger or comparable to the Li<sup>+</sup>-PS interaction, leads to Li<sub>2</sub>S<sub>x</sub> dissociation and high PS solubility.<sup>35</sup> Between the LiTDI and LiTFSI-based electrolytes, though the former has slightly more ion-pairs than the latter, the modelling suggests Li<sub>2</sub>S<sub>8</sub> to be more soluble in the latter (Table S1). This is consistent with previous studies attributing lower Li<sub>2</sub>S<sub>8</sub> solubility in LiTDI due to the large anion size as well as different solvation of LiTDI with Li<sub>2</sub>S<sub>8</sub> forming dimers, as compared to monomers or higher order polysulfides in the case of LiTFSI-based electrolytes.<sup>16,38</sup>

## Concluding Remarks

Overall, increasing the electrolyte salt concentration significantly improves the electrochemical performance of Li-S batteries. However, the salt concentration required for the improvements varies by the anion used. Weakly coordinating anions, such as TFSI and TDI, favour Li<sup>+</sup>-solvent rather than Li<sup>+</sup>-anion interactions, which renders less free solvent, which in turn leads to lower PS solubility and enhanced capacity utilization, even at moderate salt concentrations (2 m). In contrast, the Tf anion, has a stronger tendency to form aggregates, which hampers its usefulness at similar salt concentrations, but more performant LiTf-based electrolytes can be made by increasing the salt concentration even further (5 m). At the same time, global properties such as viscosity may be affected adversely, which mean that also the usage demands, for example C-rates to be used, are to be taken into account when the salt/anion choice is being made.

## Acknowledgments

As a part of the DESTINY PhD programme, this publication acknowledges funding from the European Union’s Horizon 2020 research and innovation programme under the Marie Skłodowska-



Curie Actions COFUND (Grant Agreement No-945357). The authors would also like to acknowledge the financial support from the Swedish Research Council (grant #2020-03988 & 2021-00613), the Swedish Energy Agency (project #50638-1) and VINNOVA/Batteries Sweden (grant 2019-00064). The authors thank Maciej Smoliński for the cathode preparation, funded by the ENERGYTECH-1 project granted by Warsaw University of Technology under the program Excellence Initiative: Research University (IDUB). Dr Soniya S Rao (Chalmers) is gratefully acknowledged for the DFT assistance, and Dr Tomooki Hosaka (Chalmers) is acknowledged for editing and helpful discussions.

## ORCID

Aginmariya Kottarathil  <https://orcid.org/0000-0002-8670-728X>  
 Patrik Johansson  <https://orcid.org/0000-0002-9907-117X>  
 Wladyslaw Wiczorek  <https://orcid.org/0000-0002-3881-3838>

## References

- P. G. Bruce, S. A. Freunberger, L. J. Hardwick, and J. M. Tarascon, *Nat. Mater.*, **11**, 19 (2012).
- R. Van Noorden, *Nature*, **507**, 26 (2014).
- J. B. Goodenough and K. S. Park, *J. Am. Chem. Soc.*, **135**, 1167 (2013).
- X. Ji and L. F. Nazar, *J. Mater. Chem.*, **20**, 9821 (2010).
- A. Manthiram, Y. Fu, S. H. Chung, C. Zu, and Y. S. Su, *Chem. Rev.*, **114**, 11751 (2014).
- L. F. Nazar, M. Cuisinier, and Q. Pang, *MRS Bull.*, **39**, 436 (2014).
- D. Aurbach, E. Pollak, R. Elazari, G. Salitra, C. S. Kelley, and J. Affinito, *J. Electrochem. Soc.*, **156**, A694 (2009).
- M. Zhao, B. Q. Li, X. Q. Zhang, J. Q. Huang, and Q. Zhang, *ACS Cent. Sci.*, **6**, 1095 (2020).
- J. B. Robinson et al., *J. Phys.: Energy*, **3**, 031501 (2021).
- S. Wickerts, R. Arvidsson, A. Nordelof, M. Svanstrom, and P. Johansson, *ACS Sustain. Chem. Eng.*, **11**, 9553 (2023).
- B. Lin, Y. Zhang, W. Li, J. Huang, Y. Yang, S. W. Or, Z. Xing, and S. Guo, *eScience*, **4**, 100180 (2023).
- G. Xu, B. Ding, J. Pan, P. Nie, L. Shen, and X. Zhang, *J. Mater. Chem. A*, **2**, 12662 (2014).
- G. Liu, Q. Sun, Q. Li, J. Zhang, and J. Ming, *Energy & Fuels*, **35**, 10405 (2021).
- A. Manthiram, Y. Fu, and Y. S. Su, *Acc. Chem. Res.*, **46**, 1125 (2013).
- Y. V. Mikhaylik and J. R. Akridge, *J. Electrochem. Soc.*, **151**, A1969 (2004).
- J. Chen et al., *Adv. Energy Mater.*, **6**, 1600160 (2016).
- M. He, L. X. Yuan, W. X. Zhang, and Y. H. Huang, *J. Solid State Electrochem.*, **17**, 1641 (2013).
- C. Zhang, H. B. Wu, C. Yuan, Z. Guo, and X. W. D. Lou, *Angew. Chem. Int. Ed.*, **38**, 9592 (2012).
- X. Liang, Z. Wen, Y. Liu, M. Wu, J. Jin, H. Zhang, and X. Wu, *J. Power Sources*, **196**, 9839 (2011).
- J. Hassoun and B. Scrosati, *Adv. Mater.*, **22**, 5198 (2010).
- L. Suo, Y. S. Hu, H. Li, M. Armand, and L. Chen, *Nat. Commun.*, **4**, 1481 (2013).
- T. Kobayashi, Y. Imade, D. Shishihara, K. Homma, M. Nagao, R. Watanabe, T. Yokoi, A. Yamada, R. Kanno, and T. Tatsumi, *J. Power Sources*, **182**, 621 (2008).
- C. X. Bi, L. P. Hou, Z. Li, M. Zhao, X. Q. Zhang, B. Q. Li, Q. Zhang, and J. Q. Huang, *Energy Mater. Adv.*, **4**, 0010 (2023).
- L. Cheng, L. A. Curtiss, K. R. Zavadil, A. A. Gewirth, Y. Shao, and K. G. Gallagher, *ACS Energy Lett.*, **1**, 503 (2016).
- C. Angell, C. Liu, and E. Sanchez, *Nature*, **362**, 137 (1993).
- A. Ferry, L. Edman, M. Forsyth, D. R. MacFarlane, and J. Sun, *J. Appl. Phys.*, **86**, 2346 (1999).
- K. Dokko et al., *J. Electrochem. Soc.*, **160**, A1304 (2013).
- A. Nakanishi, K. Ueno, D. Watanabe, Y. Ugata, Y. Matsumae, J. Liu, M. L. Thomas, K. Dokko, and M. Watanabe, *J. Phys. Chem. C*, **123**, 14229 (2019).
- G. Jiang, F. Li, H. Wang, M. Wu, S. Qi, X. Liu, S. Yang, and J. Ma, *Small Structures*, **2**, 2000122 (2021).
- S. Zhang, K. Ueno, K. Dokko, and M. Watanabe, *Adv. Energy Mater.*, **5**, 1500117 (2015).
- Y. Yamada, K. Furukawa, K. Sodeyama, K. Kikuchi, M. Yaegashi, Y. Tateyama, and A. Yamada, *J. Am. Chem. Soc.*, **136**, 5039 (2014).
- Y. Yamada and A. Yamada, *J. Electrochem. Soc.*, **162**, A2406 (2015).
- Y. Lin, S. Huang, L. Zhong, S. Wang, D. Han, S. Ren, M. Xiao, and Y. Meng, *Energy Storage Mater.*, **34**, 128 (2021).
- E. S. Shin, K. Kim, S. H. Oh, and W. I. Cho, *Chem. Commun.*, **49**, 2004 (2013).
- J. W. Park, K. Ueno, N. Tachikawa, K. Dokko, and M. Watanabe, *J. Phys. Chem. C*, **117**, 20531 (2013).
- M. Barghamadi, A. S. Best, A. I. Bhatt, A. F. Hollenkamp, M. Musameh, R. J. Rees, and T. Rüther, *Energy Environ. Sci.*, **7**, 3902 (2014).
- L. Niedzicki, G. Zukowska, M. Bukowska, P. Szczeciński, S. Grugeon, S. Laruelle, M. Armand, S. Panero, B. Scrosati, and M. Marcinek, *Electrochim. Acta*, **55**, 1450 (2010).
- K. S. Han et al., *Chem. Mater.*, **29**, 9023 (2017).
- Y. Yamada, J. Wang, S. Ko, E. Watanabe, and A. Yamada, *Nat. Energy*, **4**, 269 (2019).
- S. D. Han, O. Borodin, J. L. Allen, D. M. Seo, D. W. McOwen, S. H. Yun, and W. A. Henderson, *J. Electrochem. Soc.*, **160**, A2100 (2013).
- D. Zheng, X. Zhang, C. Li, M. E. McKinnon, R. G. Sadok, D. Qu, X. Yu, H. S. Lee, X. Q. Yang, and D. Qu, *J. Electrochem. Soc.*, **162**, A203 (2014).
- A. Klamt, V. Jonas, T. Bürger, and J. C. Lohrenz, *J. Phys. Chem. A*, **102**, 5074 (1998).
- A. Klamt, *Wiley Interdiscip. Rev. Comput. Mol. Sci.*, **1**, 699 (2011).
- S. Jeschke and P. Johansson, *Batteries & Supercaps*, **4**, 1156 (2021).
- COSMOtherm C3.0, release 15.01. Leverkusen, Germany: Cosmologicmbh&co. kg; 2014. <http://www.cosmologic.de>.
- TURBOMOLE V7.2 2017, a development of University of Karlsruhe and Forschungszentrum Karlsruhe GmbH, 1989-2007, TURBOMOLE GmbH, since 2007; available from <http://www.turbomole.com>.
- J. P. Perdew, *Phys. Rev. B*, **33**, 8822 (1986).
- A. D. Becke, *Phys. Rev. A*, **38**, 3098 (1988).
- D. Brouillette, D. E. Irish, N. J. Taylor, G. Perron, M. Odziemkowski, and J. E. Desnoyers, *Phys. Chem. Chem. Phys.*, **4**, 6063 (2002).
- D. M. Seo, O. Borodin, S. D. Han, Q. Ly, P. D. Boyle, and W. A. Henderson, *J. Electrochem. Soc.*, **159**, A553 (2012).
- W. A. Henderson, *J. Phys. Chem. B*, **110**, 13177 (2006).
- W. Huang, R. Frech, and R. A. Wheeler, *J. Phys. Chem.*, **98**, 100 (1994).
- J. Scheers, L. Niedzicki, G. Z. Zukowska, P. Johansson, W. Wiczorek, and P. Jacobsson, *Phys. Chem. Chem. Phys.*, **13**, 11136 (2011).
- P. Jankowski, M. Dranka, G. Z. Zukowska, and J. Zachara, *J. Phys. Chem. C*, **119**, 9108 (2015).
- L. Suo, F. Zheng, Y. S. Hu, and L. Chen, *Chin. Phys. B*, **25**, 016101 (2015).
- D. W. McOwen, S. A. Delp, E. Paillard, C. Herriot, S. D. Han, P. D. Boyle, R. D. Sommer, and W. A. Henderson, *J. Phys. Chem. C*, **118**, 7781 (2014).
- T. R. Jow, K. Xu, O. Borodin, and M. Ue, *Electrolytes for Lithium and Lithium-Ion Batteries* (Springer) vol 58 (2014).
- C. Schreiner, S. Zugmann, R. Hartl, and H. J. Gores, *J. Chem. Eng. Data*, **55**, 1784 (2010).
- T. Tsurumura, Y. Hashimoto, M. Morita, Y. Umebayashi, and K. Fujii, *Anal. Sci.*, **35**, 289 (2019).
- F. Lundin, L. Aguilera, H. W. Hansen, S. Lages, A. Labrador, K. Niss, B. Frick, and A. Matic, *Phys. Chem. Chem. Phys.*, **23**, 13819 (2021).
- D. M. Seo, O. Borodin, D. Balogh, M. O'Connell, Q. Ly, S. D. Han, S. Passerini, and W. A. Henderson, *J. Electrochem. Soc.*, **160**, A1061 (2013).
- M. Forsyth, H. Yoon, F. Chen, H. Zhu, D. R. MacFarlane, M. Armand, and P. C. Howlett, *The Journal of Physical Chemistry C*, **120**, 4276 (2016).
- M. Callsen, K. Sodeyama, Z. Futera, Y. Tateyama, and I. Hamada, *The Journal of Physical Chemistry B*, **121**, 180 (2017).
- K. Dokko, D. Watanabe, Y. Ugata, M. L. Thomas, S. Tsuzuki, W. Shinoda, K. Hashimoto, K. Ueno, Y. Umebayashi, and M. Watanabe, *J. Phys. Chem. B*, **122**, 10736 (2018).
- K. Ueno, J. W. Park, A. Yamazaki, T. Mandai, N. Tachikawa, K. Dokko, and M. Watanabe, *J. Phys. Chem. C*, **117**, 20509 (2013).
- H. Pan, X. Wei, W. A. Henderson, Y. Shao, J. Chen, P. Bhattacharya, J. Xiao, and J. Liu, *Adv. Energy Mater.*, **5**, 1500113 (2015).